Int J Adv Manuf Technol (2017) 93:1699–1714
DOI 10.1007/s00170-017-0646-x

ORIGINAL ARTICLE

In-process endpoint detection of weld seam removal in robotic abrasive belt grinding process

Vigneashwara Pandiyan[1] · **Tegoeh Tjahjowidodo**[1]

Received: 5 September 2016 / Accepted: 5 June 2017 / Published online: 21 June 2017
© Springer-Verlag London Ltd. 2017

Abstract This paper proposes a novel approach for in-process endpoint detection of weld seam removal during robotic abrasive belt grinding process using discrete wavelet transform (DWT) and support vector machine (SVM). A virtual sensing system is developed consisting of a force sensor, accelerometer sensor and machine learning algorithm. This work also presents the trend of the sensor signature at each stage of weld seam evolution during its removal process. The wavelet decomposition coefficient is used to represent all possible types of transients in vibration and force signals generated during grinding over weld seam. "Daubechies-4" wavelet function was used to extract features from the sensors. An experimental investigation using three different weld profile conditions resulting from the weld seam removal process using abrasive belt grinding was identified. The SVM-based classifier was employed to predict the weld state. The results demonstrate that the developed diagnostic methodology can reliably predict endpoint at which weld seam is removed in real time during compliant abrasive belt grinding.

Keywords Abrasive belt grinding · DWT · Surface finish/integrity · SVM · Weld seam removal

1 Introduction

Welding is an inevitable process during manufacturing of aerospace components such as turbine blade [1, 2]. Weld seam that is produced during the manufacturing cycle of these components needs to be removed. Aerospace components operating in harsh environments, with high temperature, high pressure and at high speed must have high surface integrity and profile precision. Abrasive belt grinding has been a potential choice in removing weld seam in industries. Axinte et al. [3] have established that belt grinding process has the ability to eliminate the machining marks and to establish a required surface quality. High material removal rate with acceptable surface quality can be achieved through belt grinding processes. It is acknowledged by the workforce as a tertiary finishing process and does not necessitate extra corrective work before and after [4]. Current industrial practice in removing weld seam involves a manual belt grinder, either pneumatic or electric, where flat spots are created in and around neighbouring surfaces of the weld and finally removed by the operator. Such a process is laborious as the operator has to appropriately define the grinding paths for free-form workpieces during the weld seam removal process. A manual belt grinding process is also time consumptive as the part has to be taken from robot cell to the manual machining station and vice versa. An automated tracked weld shaving system has been commercially available, but the problem with such a system is that it requires rather extensive time for assembling and dis-assembling [5]. Though finishing is done using belt grinders with robot manipulators in a highly sophisticated machining cell, the industry still depends primarily on skilled operators in removing weld seam using belt sanders manually. For ensuring a fully automated time-intensive weld seam removal work, it is necessary to build a predictive system that can monitor the weld seam removal in real time. This approach will also improve the production process quality by reducing unnecessary costs and increasing the level of safety. A reliable in-process monitoring system will transform thee manufacturing environment from manually operated production machines to unsupervised robotic machining

✉ Tegoeh Tjahjowidodo
ttegoeh@ntu.edu.sg

[1] School of Mechanical and Aerospace Engineering, Nanyang Technological University, Singapore 639798, Singapore

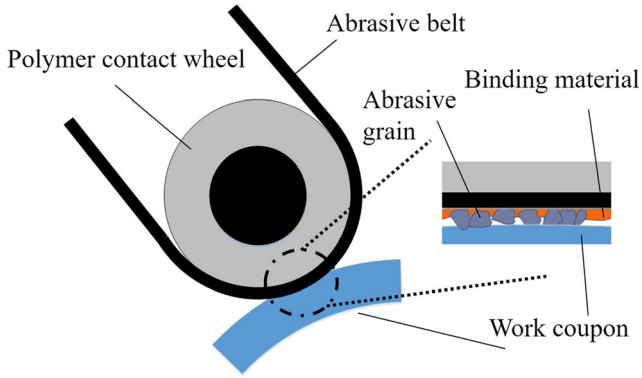

Fig. 1 Principle of belt grinding process

centres, which is significant in a manufacturing domain. To realise real-time monitoring of a manufacturing process, sensors are required that can serve as a feedback to the process. The sensitivity of the measurement depends on the selection of sensors and their placement at the suitable location [6, 7]. A vision sensor has been extensively used in sensing the initial weld point, thus providing weld seam information for assistance to the welding robot [8, 9]. The way by which various sensors are incorporated into the operation of the system is usually a major factor in the overall design of an intelligent system [10, 11]. Pandiyan et al. [12] have developed a real-time multi-sensor integration system to predict surface roughness of the work coupon in the belt grinding process based on contact conditions using an SVM-based classification algorithm, while Kanish et al. [13] utilised a fuzzy inference system (FIS) to respond to the same problem. Wavelet transform has a superior resolution in the time–frequency domain so that it can find more evidence in the time domain at various frequency bands [14–16]. Wavelet transform utilises an evaluating wavelet function that is localised in both frequency and time to identify transient changes in the sensor signals in the time domain [17]. Nurprasetio et al. [18] developed a novel method for machinery fault identification based on the combination of minimum distance pattern recognition technique and feature vectors based on the DWT decomposition. Wavelet transformation is an excellent tool to characterise dynamic signals as it analyses signals into different packages of energy. From the classification point of view, wavelet transformation is a good contender for organising a very characteristic data set for cutting force signatures [19]. Saravanan and Ramachandran [20] developed a pattern classification algorithm for fault diagnostics of a spur bevel gear box using discrete wavelet transform based on vibration signal. Theoretical models are very complicated to develop because of the inadequate understanding of machining processes [21]. The decision-making process used signal features to accomplish the pattern association assignment by bracketing the signal feature to the appropriate class. SVM has the capability to deal with large feature space because the training of SVM is carried out so that the dimension of classified vectors does not have an individual effect on the functioning of SVM as it has on the performance of standard classifiers. That is why it is proficient in the classification of large feature space [22]. Caldas and Ekici [23] have stated that the ANN model has smaller prediction accuracy and also involves more computational time than SVM. The support vector machine fabricates a separating hyperplane amplifying the margin between two data sets according to their classes which have been formerly mapped to a high-dimensional space by using a kernel function [24, 25].

In this research, we have developed a real-time endpoint prediction system for weld seam removal during the abrasive belt grinding process with the help of accelerometer sensor, force sensor, and SVM-based machine learning classification algorithm. The paper is organised as follows: the problem statement is presented in Sect. 1, followed by a brief overview of abrasive belt grinding process, DWT, and SVM in Sect. 2. The proposed methodology, machining conditions, weld seam geomentry evolution, implementation of multi-sensor integration, and sensor signature analysis are outlined in Sect. 3. Wavelet decomposition-based feature extraction and SVM-based endpoint detection are elaborated in Sect. 4. Validation of the proposed methodology is detailed in Sect. 5. Finally, the conclusions of this research work are summarised in Sect. 6.

2 Theoretical basis

2.1 Abrasive belt grinding

Abrasive belt grinding is a modification of the traditional grinding processes where the outer layer of the contact wheel is made of soft materials. The grinding belt is made up of coated abrasives and is fastened around at least two rotating

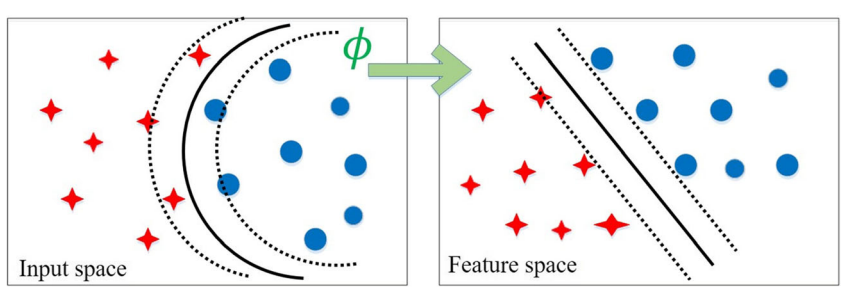

Fig. 2 Mapping the input space to feature space using kernel trick

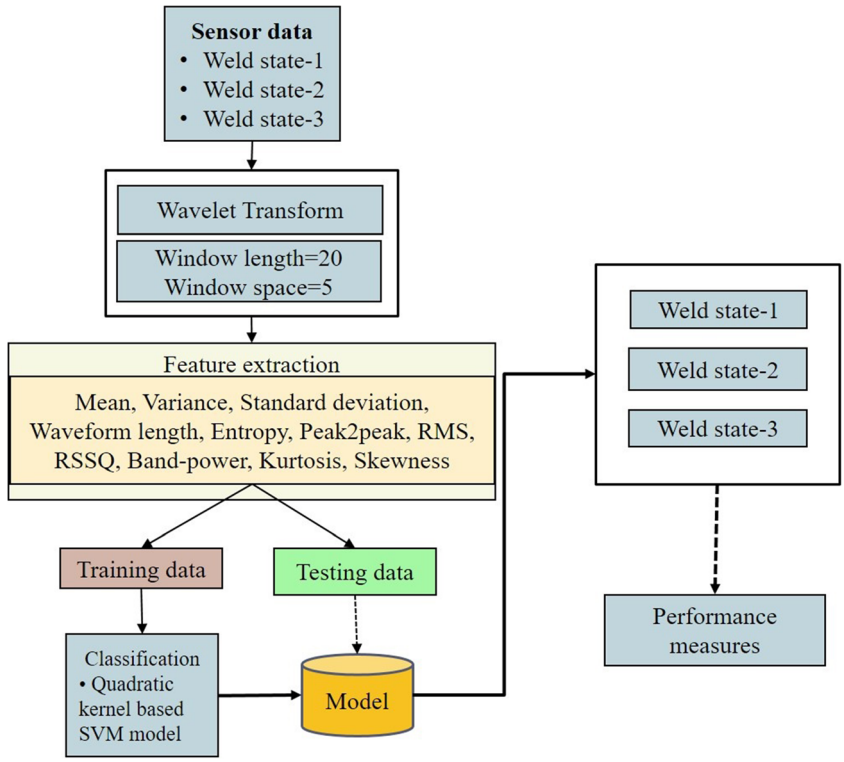

Fig. 3 General description of the proposed methodology

rubber contact wheels which makes it a compliant tool. The soft contact rubber wheel enables this machining process to appropriately manufacture free-form surfaces due to its capability to adapt to the workpiece surface [26]. The major benefit of this process is the use of a compliant wheel body and an abrasive film which can be regenerated automatically [27] as shown in Fig. 1. The non-linear behaviour of the belt grinding tool is predominantly dependent on the contacts between the workpiece and the abrasive belt. Similar to other abrasive machining processes, many machining parameters are impacting the final ground surface quality, including the grinding belt topography features and cutting parameters. The cutting parameters include belt speed, feed rate, workpiece geometry and belt preloaded tension, while belt topography features include the information such as grit size, grain distance and wear rate [4]. Understanding of such a process is one of the challenging problems in the industry due to the high complexity and non-linearity. Although super finishing by belt grinding is straightforward and inexpensive, important aspects of the belt grinding process are not well grasped, and hence used in industries based on empirical rules. Cutting force and tool vibration signals change when the pressure distribution of the polymer backing varies based on the interaction with the workpiece geometry which can be suitably exploited to predict the contact conditions.

Table 1 Parameters used in the belt grinding experimental trials

Parameter	Value
Belt grinding speed	18 m/s
Contact wheel diameter	16 mm
Hardness of contact wheel (polyurethane)	80 Duro
Lubrication	Dry
Feed	30 mm/s
Belt finishing duration	Variable
Operational mode	Position control

2.2 Discrete wavelet transform

The wavelet transform is specially adapted for the detection of transient signals, i.e. signal components that last a short period

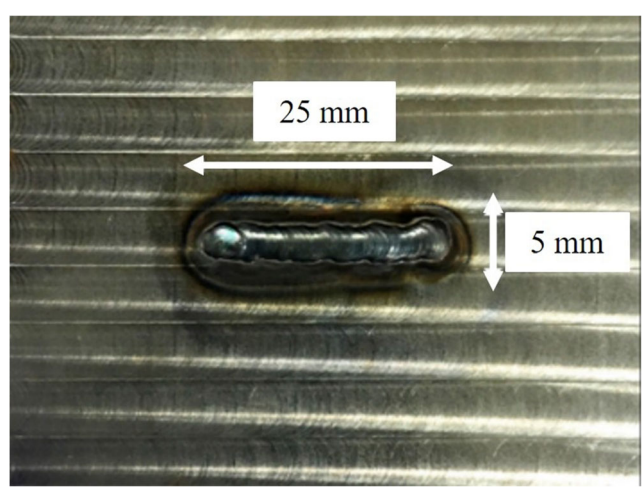

Fig. 4 Weld seam of the mild steel coupon

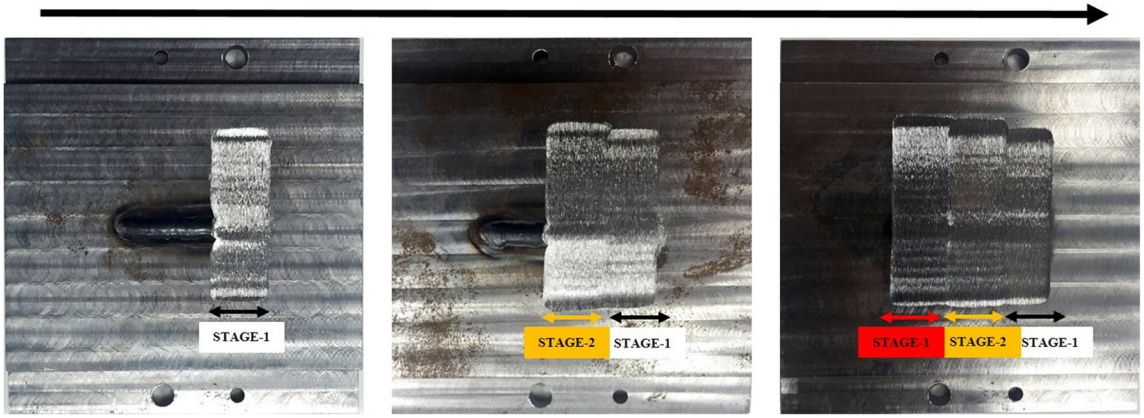

Fig. 5 Stage-wise weld seam removal from workpiece surface in dry conditions

and span a wide frequency range [28]. The main advantage of the wavelet transform is that it allows outstanding localisation in both the frequency and time domain via dilations and translations of the mother wavelet. Continuous wavelet transform

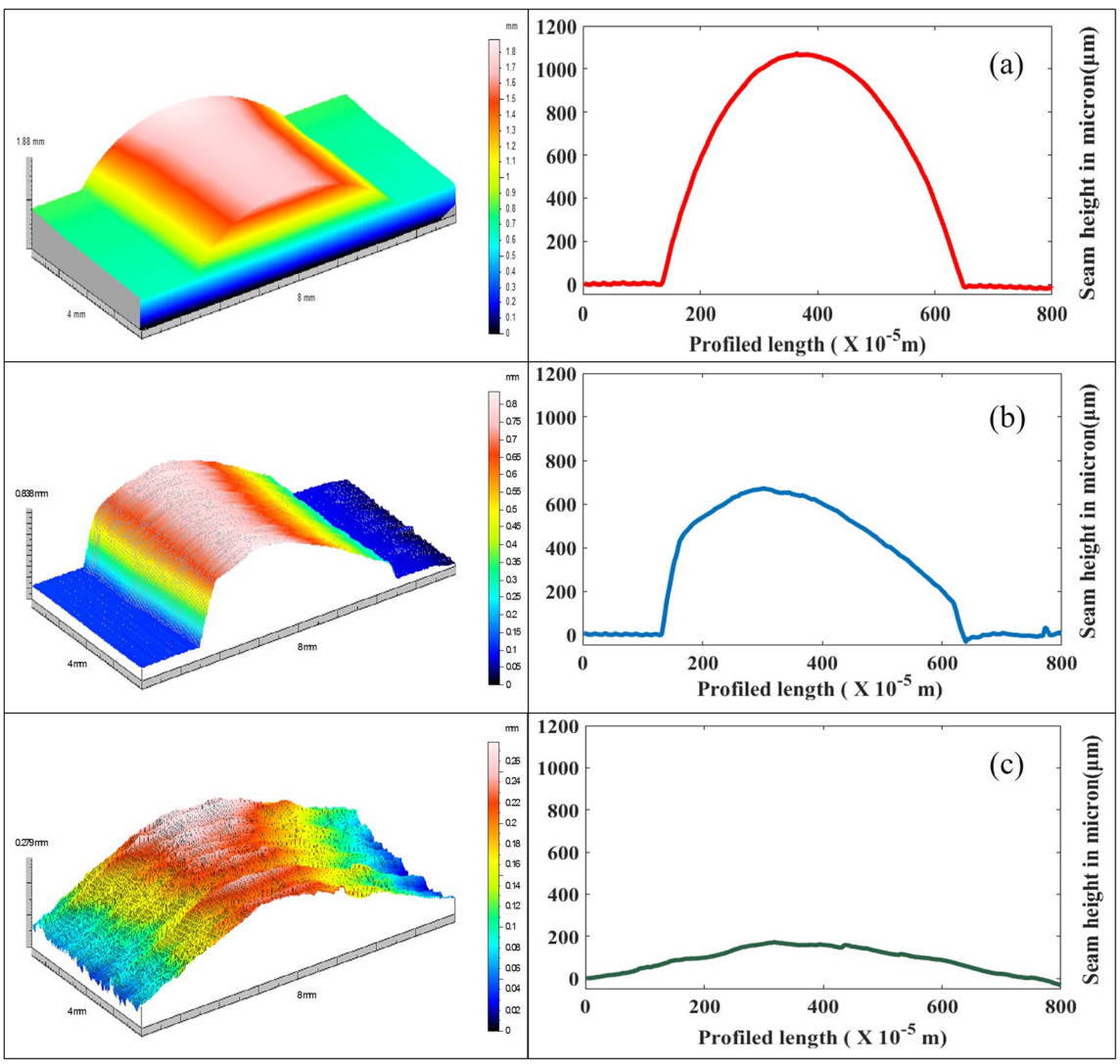

Fig. 6 **a** 3D and 2D profile extracted from the weld seam before belt grinding process. **b** 3D and 2D non-symmetrical profile extracted from the weld seam after consecutive passes of belt grinding process (state 1). **c** 3D and 2D profile extracted when the weld seam is distinctively removed (state 2)

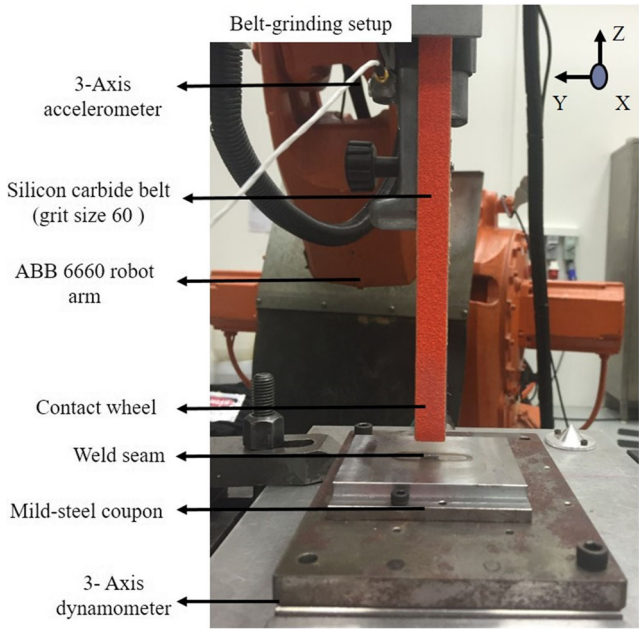

Fig. 7 Multi-sensor belt grinding setup

(CWT) of $f(t)$ can be defined mathematically in a time-scale approach of signal processing as

$$\mathrm{CWT}(i,j) = \frac{1}{\sqrt{|i|}}\int_{-\infty}^{\infty} f(t)\Psi^*\left(\frac{t-j}{i}\right)dt \tag{1}$$

where $\Psi(t)$ denotes the mother wavelet, parameter i denotes the reciprocal of frequency and parameter j directs the translation. Discrete wavelet transform is a type of the wavelet transform operation using a distinct set of the wavelet scales (frequency) and translations. It conforms some distinct guidelines that decompose the signal into a mutually orthogonal set of wavelets. The translation and dilation operations applied to the mother wavelet are implemented to determine the wavelet coefficients, which corresponds to the relationship between the wavelet and a localised section of the signal. Discrete wavelet transform is derived from the discretisation of CWT(i, j) as given by

$$\mathrm{DWT}(x,y) = \frac{1}{\sqrt{2^x}}\int_{-\infty}^{\infty} f(t)\Psi^*\left(\frac{t-2^x y}{2^x}\right)dt \tag{2}$$

where i and j are replaced by 2^x and $2^x y$. Discrete wavelet transform analysis breaks the signal into several components covering the complete frequency spectrum with various bandwidths. Discrete wavelet transform coefficients can be obtained by filter-bank structure using the Mallat (pyramidal) algorithm [29]. The approximation coefficients at subsequent lower levels are passed through a high-pass and a low-pass filter. The frequency bands of the filters are based on the sampling frequency (fs) and the upmost band, which relates to a level-one decomposition, covering between $fs/2$ to $fs/4$. This is followed by a downsampling by 2 to calculate both the detail coefficients (of the high-pass filter) and the approximation coefficients (of the low-pass filter) at a next decomposition level.

2.3 Support vector machines

The support vector machine constructs a separating hyperplane increasing the margin between distinct data sets according to their classes which have been formerly mapped to a high-dimensional space [30]. For linearly distinguishable data, a hyperplane $f(\mathrm{x}) = 0$ which separates the feature space can be determined as

$$f(\mathbf{x}) = \mathbf{w}^{\mathbf{T}}\mathbf{x} + b = \sum_{i=1}^{n} \alpha_i \mathbf{x_i}^{\mathbf{T}}\mathbf{x} + b \tag{3}$$

where $\mathbf{w} = \sum_{i=1}^{n} \alpha_i x_i$ is an n-dimensional vector and b is a scalar; the vector $\mathbf{w}$ and the scalar b determine the optimal separating hyper-plane that creates the utmost distance amid the plane and the nearest data. The non-linear classification problems can also be resolved by using SVM applying a kernel trick [24]. Linear classification can be derived from the non-linear SVM by implicitly mapping the input space $\mathcal{X}$ to a feature space $\mathcal{F}$ as shown in the Fig. 2 using a non-linear function $\phi : \mathcal{X} \rightarrow \mathcal{F}$ and training the SVM for the mapped features $\phi(\mathbf{x})$. In the space $\mathcal{F}$, the discriminant function is

$$f(\mathbf{x}) = \mathbf{w}^{\mathbf{T}}\phi(\mathbf{x}) + b = \sum_{i=1}^{n} \alpha_i \phi(\mathbf{x_i})^T \phi(\mathbf{x_j}) + b \tag{4}$$

$$f(\mathbf{x}) = \sum_{i=1}^{n} \alpha_i K(\mathbf{x_i}, \mathbf{x_j}) + b \tag{5}$$

Non-linear SVMs can then be trained by replacing the inner products in (4) with the corresponding kernel function $K(\mathbf{x_i}, \mathbf{x_j}) = \phi(\mathbf{x_i})^{\mathbf{T}}\phi(\mathbf{x_j})$. The resulting non-linear SVM-kernelised function can be represented as in (5). Based on the authors' knowledge, the application of a wavelet transform for real-time weld seam endpoint detection using multiple sensor signatures in the belt grinding process has never been addressed in the literature. Later, the experimental results show that the proposed system possesses reliability for detection of the weld seam states by employing a machine learning algorithm based on SVM.

3 Proposed methodology and experimental setup

3.1 Methodology

Weld seam of three different removal states is machined with an abrasive belt with the same grinding condition. The signatures during machining of different weld seam states are

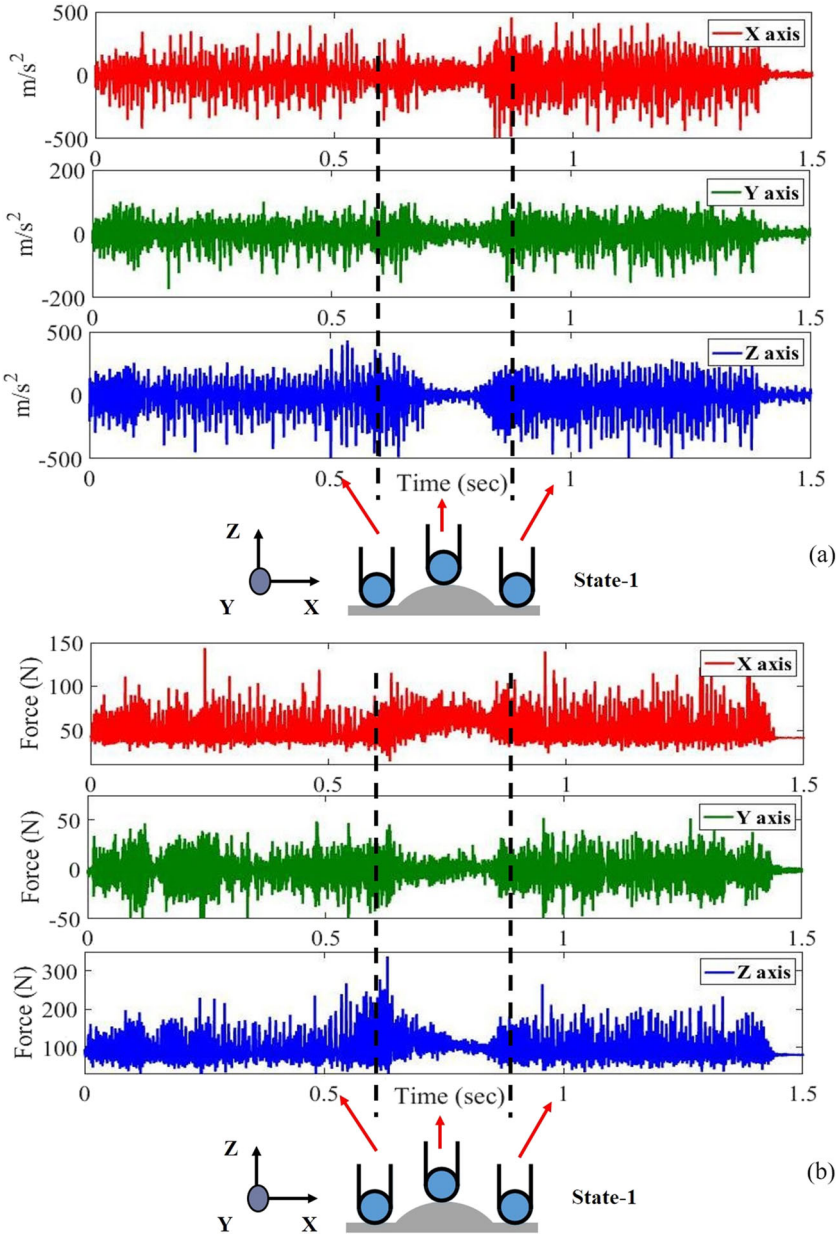

Fig. 8 **a** Accelerometer signatures obtained on contact of the belt grinding arm over non-symmetrical weld seam profile state 1. **b** Force signatures obtained on contact of the belt grinding arm over non-symmetrical weld seam profile state 1

captured using an appropriate force and an accelerometer with a sampling rate of 2 kHz. The wavelet transform is used to represent all possible types of momentary variation in vibration and force signals generated during grinding of three weld seam states. The Daubechies-4 (Db4) wavelet function was used to extract features from vibration signal with a window size of 20 and spacing of the window of 5. The eight-level wavelet decomposition features based on DWT coefficients such as mean, variance, standard deviation, waveform length, entropy, peak2peak, root mean square (RMS), root sum of squares (RSSQ), band power, kurtosis, and skewness is extracted from the force and vibration signal. Once the features are extracted, the supervised learning technique based on SVM using quadratic kernel function is used to create a classification model. Three weld seam conditions were used as the data input for SVM training and testing process. The SVM classification was performed in MATLAB classification learner toolbox. After the model is trained, a new feature set of signatures is extracted from the weld seam states 1, 2, and 3 with the same machining condition. These wavelet decomposition features are passed into the classification model developed and trained using SVM to check the accuracy of the model. Schematic representation of the methodology is described in Fig. 3.

3.2 Experimental setup and grinding conditions

The belt grinder used in the experimental trials is an electrically powered abrasive belt tool that runs at 11,000 rpm

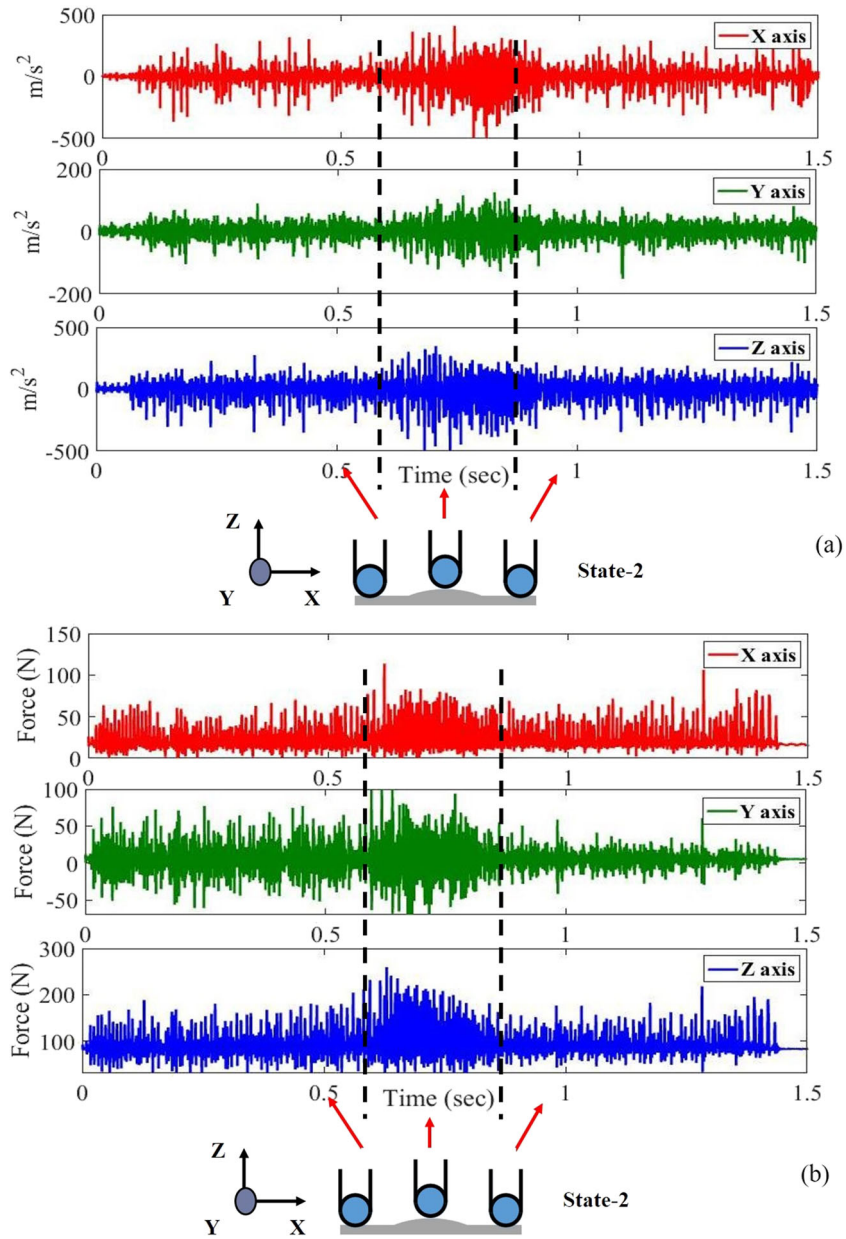

Fig. 9 **a** Accelerometer signatures obtained on contact of the belt grinding arm over weld seam profile state 2. **b** Force signatures obtained on contact of the belt grinding arm over weld seam profile state 2

at unloading condition and can drive belts with dimensions about 3/4″ wide × 18″ long. The electric belt grinder is integrated with a multi-degree industrial ABB 6660-205-193 robot as a manipulator such that a manufacturing cell is established for the weld seam removal process. The robot manipulator arm is primarily used for toolpath planning and control. The contact wheel of the belt grinder head is kept at a normal angle to the machined surface to maintain steady contact throughout grinding. Belt wear effect was ignored during the experimental trials as the trials were conducted in the useful lifetime of the belt tool. Machining was performed with abrasive belts of grit size 60 made up of silicon carbide abrasive and the contact wheel rubber backing material having a hardness of 80 Duro. Closed-loop control was accomplished by giving feedback to the robot controller relating to the position of the grinding point. Weld seam specimens were grinded with the process parameters as shown in Table 1 for all the experimental trials.

3.3 Weld seam removal

Weld seams are made up of stainless steel (SUS308) filler rod on mild steel work coupons using tungsten inert gas welding with argon as the inert gas. To ensure the reproducibility of the removal process, weld seams of dimension 25 mm × 5 mm × 1.2 mm (L × B × H) are prepared on a flat mild steel work coupons as shown in Fig. 4.

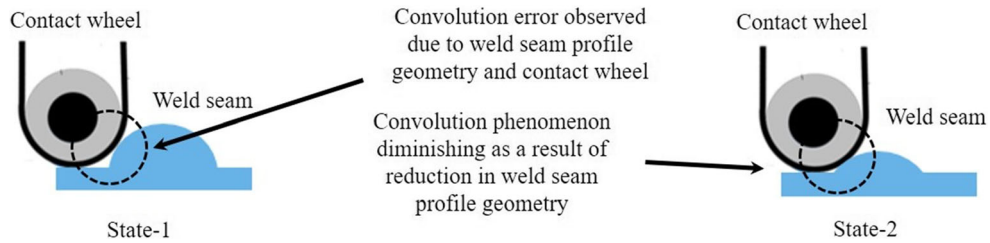

Fig. 10 Comparison of the convolution error during machining weld seam in states 1 and 2 with the contact wheel

Since the weld seam is of length 25 mm and the contact width of the belt cross section is 9 mm, tool path planning is divided into three stages for complete weld removal from the surface of the work coupon with each stage removing one third of the weld seam length as shown in Fig. 5. For each and every pass on the weld seam, the weld seam profile height depletes, and the weld seam is completely removed. Tooling passes are done perpendicular to the length of the weld seam which helps to remove the weld seam and secure the surface integrity of the adjacent area near the weld seam as shown in Fig. 5 below.

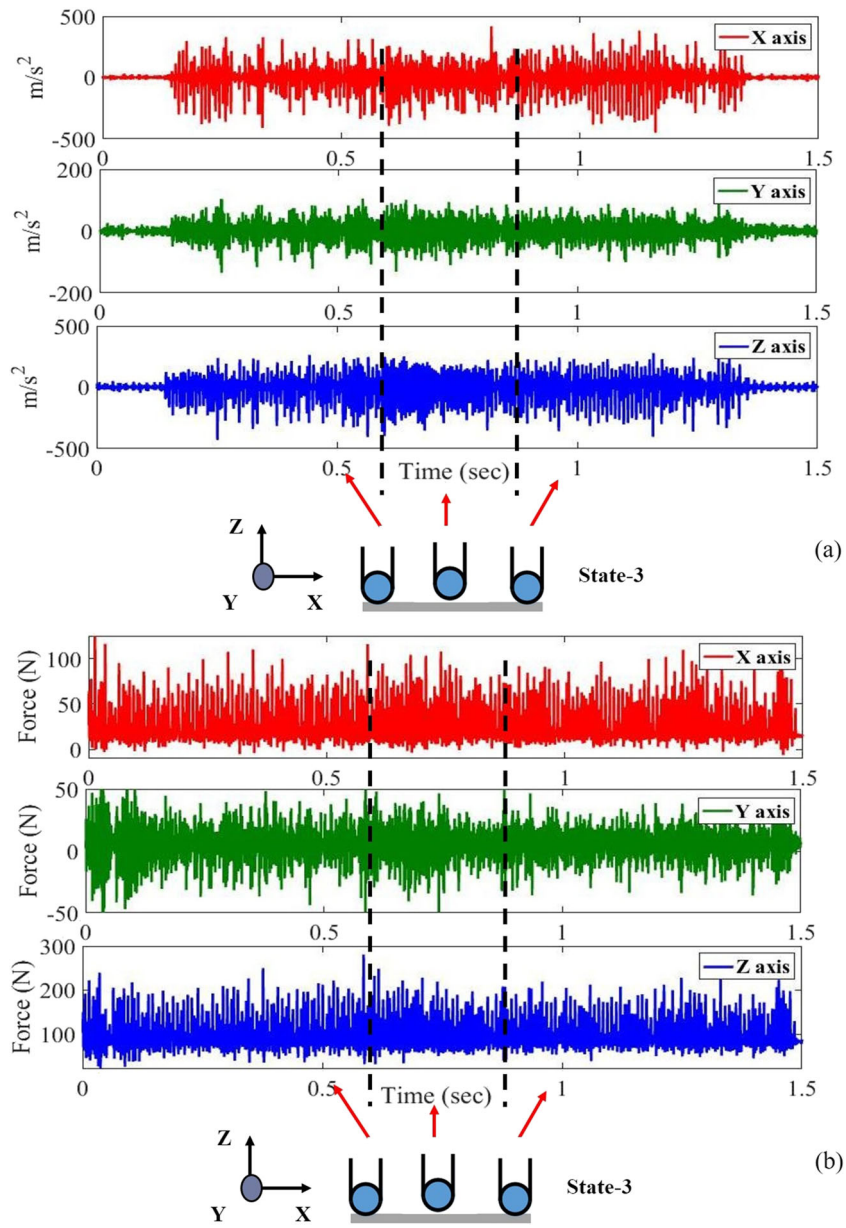

Fig. 11 **a** Accelerometer signatures obtained on contact of the belt grinding arm over completely removed weld state 3. **b** Sensor signatures obtained on contact of the belt grinding arm over completely removed weld state 3

Table 2 Wavelet frequency bands for experimental trials

Decomposition level	Frequency band (Hz)
Level 1	1000–500
Level 2	500–250
Level 3	250–125
Level 4	125–62.5
Level 5	62.5–31.25
Level 6	31.25–15.625
Level 7	15.625–7.825
Level 8	7.825–3.90

3.4 Evolution of weld seam geometry during belt grinding

Evolution of weld seam can be categorised as three distinct states and is completely dependant on the geometry of the contact wheel of the belt grinder. The three states of weld seams are categorised by their geometry of the scanned profile using a Taly-scan profilometer. The shape of the weld seam profile before machining is symmetrical on either side as shown in Fig. 6a.

The weld profile looks hemispherical with its peak at the centre. State 1 includes a weld profile evolved as a result of grinding which is not symmetrical in shape with an apparent reduction in height compared to the weld profile obtained at the initial state as shown in Fig. 6b. Such a weld profile evolution can be attributed to the convolution error caused by the contact wheel diameter and inclination between the weld seam and the contact wheel of the grinder. The highest point of the profile is skewed towards the direction where the initial contact is made by the grinding wheel on the weld seam on each and every pass. State 2 is where the weld seam is distinctively removed, and there is also a reduction in the breadth of the weld seam as a result of continuous grinding as shown in Fig. 6c. The contact wheel of the belt does not have convolution problem during the grinding process as it was subjected to in state 2. State 3 is the final state where the weld seam is completely removed. This research tries to predict state 3 of the weld seam virtually based on sensor signatures.

3.5 Complementary based multi-sensor integration system

A complementary multi-sensor integration system comprising an accelerometer and force sensor was developed and proposed as a strategy to estimate the state of the weld seam removal. A Kistler 8763A500 triaxial accelerometer is placed near the tension arm of the electric belt grinder to obtain data on tool vibration during machining. The accelerometer is placed on the tool in such a way that it does not interrupt the belt transmission. Kistler 9254, a three-component dynamometer, is positioned below the work coupon to measure the forces generated during grinding. Figure 7 shows the overall experimental setup and sensor placement. The sensor position and data sampling rate of 2 kHz were kept constant throughout the experiment for both accelerometer and force sensor. A data acquisition device supported by DEWESoft platform is used to acquire and post-process the measured signal from both sensors.

3.6 Sensor signature analysis for different weld seam profile states

A successful weld seam endpoint detecting method must be responsive to the change in contact condition, i.e. change in profile geometry of the weld seam on each and every pass. Based on visual observation, the signatures from the multi-component dynamometer on each pass suggest that forces along X (along with the direction of the pass), Z (normal to the work coupon surface) and Y (perpendicular to the pass) show evident

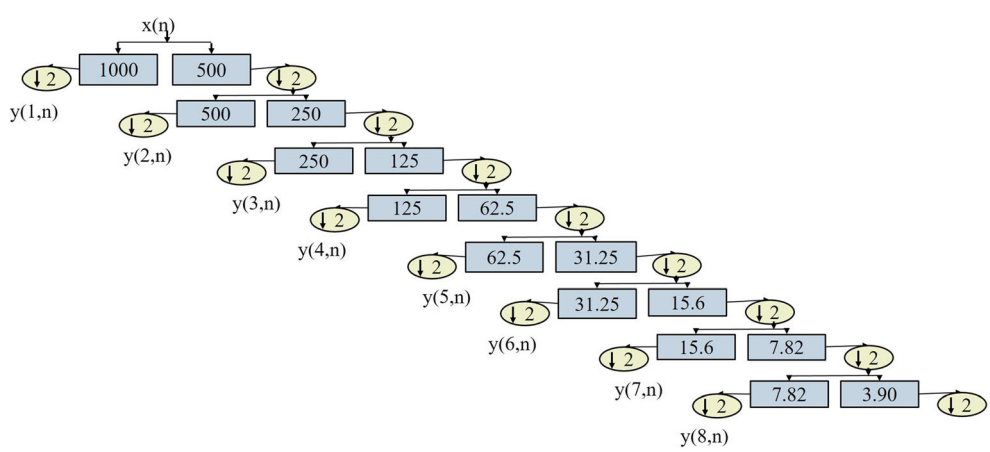

Fig. 12 Wavelet tree decomposition with eight detail levels of time signal

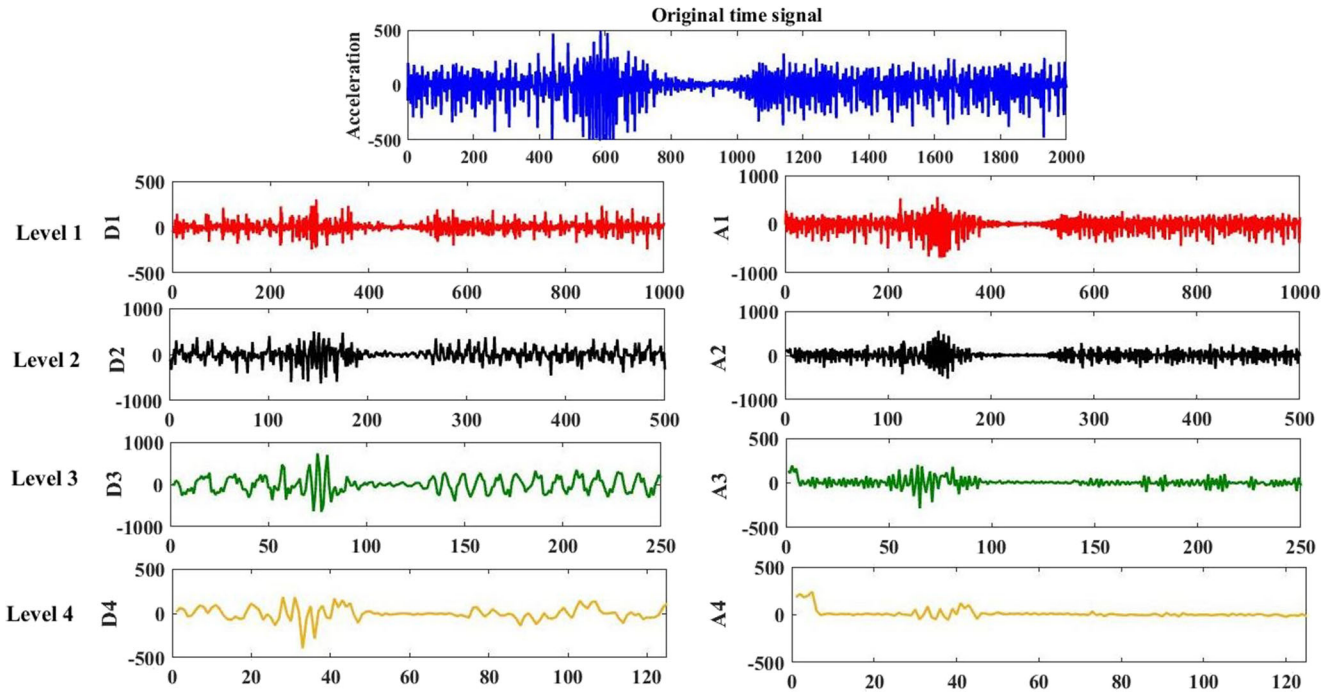

Fig. 13 Wavelet decompositions for time signal obtained from accelerometer during grinding of weld state 1

significance. The same finding is also observed from the accelerometer sensor signatures in all the three axes. An accelerometer sensor is subjected to noise during data acquisition as it is mounted on the grinding arm. Dominant frequency noise components acquired are eliminated using Butterworth bandstop filter after data acquisition.

For detecting the weld seam states efficiently in the belt grinding process, monitoring signatures from the force and accelerometer signal is essential. Analysing sensor

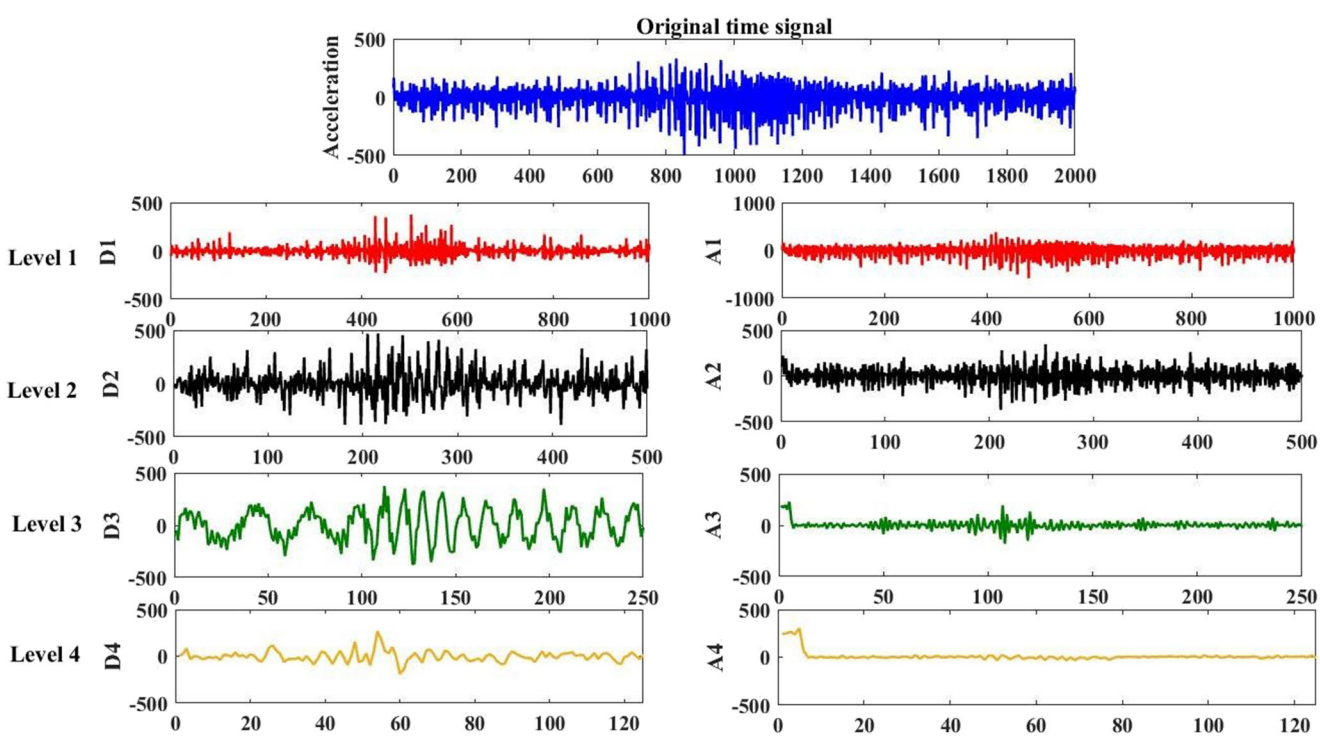

Fig. 14 Wavelet decompositions for time signal obtained from accelerometer during grinding of weld state 2

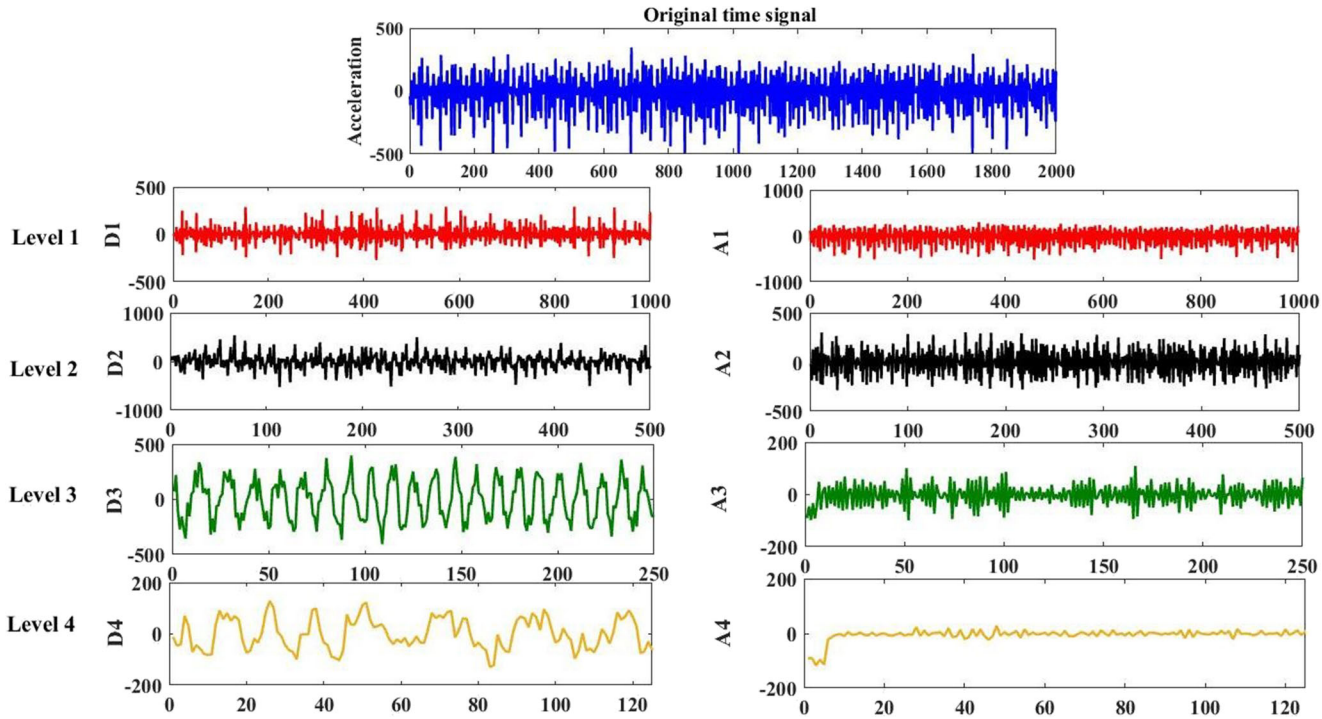

Fig. 15 Wavelet decompositions for time signal obtained from accelerometer during grinding of weld state 3

readings during the grinding process of the weld seam at state 1, it was evident that there is a reduction in the magnitude of the signatures for both the sensor in all the axes when the grinder encounters the weld profile. Accelerometer and force sensor signatures on all three axes, when the contact wheel of the belt grinder encounters with the weld seam in state 1, are shown in Fig. 8. Figure 9 shows the sensor signatures acquired during the grinding process of the weld seam in state 2. As the contact wheel of the belt grinder encounters the weld profiles at state 2, where the height of the seam has been reduced, there is an increase in the magnitude of the signatures. The increase in the magnitude of the signatures is attributed to the fact that the grinding contact wheel made complete contact over the weld seam and did not encounter any convolution error (see Fig. 10 for illustration). However, in weld state 3, the signatures appear to be constant throughout the belt grinding process as the weld seam is completely removed as shown in Fig. 11. Vibration and force sensor signals, unlike weld seam states 1 and 2, do not show any signal transitions throughout in state 3.

4 Endpoint detection of weld seam removal

4.1 Wavelet decomposition

This work employs the orthogonal Daubechies filters of length 4 and is applied to extract the wavelet coefficients of discrete time signals. Table 2 shows the frequency bands covered by the eight decomposition levels in the performed experiments. The sensor signals from 60 experimental trials conducted using the same belt grinding condition are then decomposed up to eight levels taking Daubechies-4 mother wavelet for extraction of features. The frequency bandwidths of approximation and detail coefficients of wavelet decompositions are shown in Fig. 12.

Figure 13 shows the acceleration response in state 1 when the weld seam has an asymmetrical profile and the corresponding approximation and detail coefficients

Table 3 Features extracted based on wavelet decomposition coefficients

Feature number	Feature name
Feature 1	Mean
Feature 2	Variance
Feature 3	Standard deviation
Feature 4	Waveform length
Feature 5	Entropy
Feature 6	Peak2peak
Feature 7	Root mean square (RMS)
Feature 8	Root sum of squares (RSSQ)
Feature 9	Band power
Feature 10	Kurtosis
Feature 11	Skewness

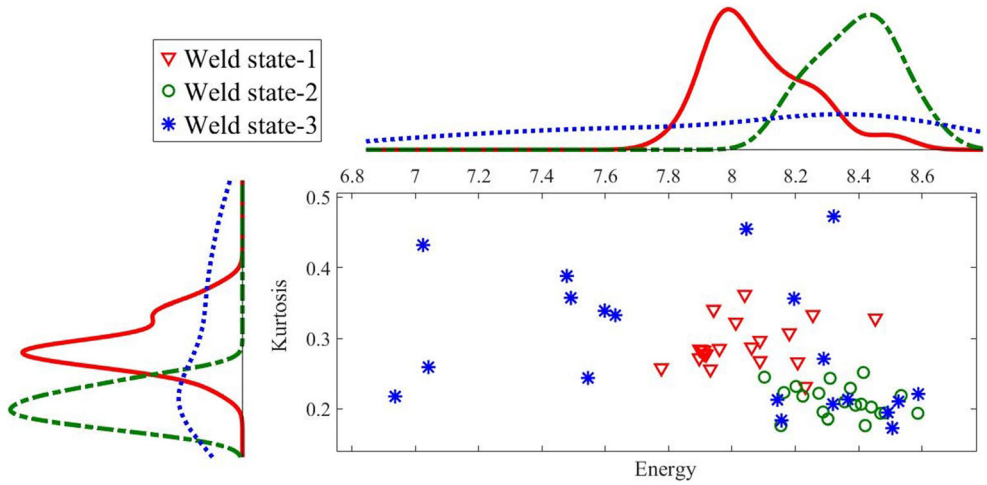

Fig. 16 Relationship and distribution between kurtosis and energy feature acquired from accelerometer signal for level 1 decomposition for three different weld seam states

obtained by DWT up to four levels. The acceleration time signals of weld seam profile in state 2 and state 3 and their four-level decomposition into approximation and detail coefficients are shown in Figs. 14 and 15. The sensor signals obtained during grinding different states of weld seam profile geometry are distinct in wavelet decompositions when they are compared with each other. The above finding reveals DWT can be used as an effective tool for detecting weld seam removal during the compliant belt grinding process.

4.2 Wavelet-based feature extraction

Fundamental to the success of classification and endpoint detection of the weld seam removal problem is the extraction of a set of informative features that provides the best descriptive information about the content of the input signals. Features providing more details about the signal are generated based on wavelet coefficients in the frequency sub-band when DWT is applied as discussed in Sect. 4.1.

Table 4 Support vector machine training parameters

SVM parameters	Values
Type of analysis	Classification
Validation method	Hold-out validation
SVM kernel function	Quadratic
Kernel scale	Automatic
Features	528
Classifiers	3 (weld states 1, 2 and 3)
Multiclass method	One-vs-one
Standardised data	True
Training set	70%
Testing set	30%

The features should preserve the weld seam state distinguishable as much as possible. The 11 features which are computed using all the coefficients of the details and the final approximation from sensor signatures obtained during grinding of a different weld seam profile that maximises weld state separability used in this research is listed in Table 3.

A full tree at eight decomposition levels yields 88 features, as 11 types of feature are extracted at each level. Features extracted from force and accelerometer along the three-axis channel is concatenated to form one large vector space of 528 features that will be used for endpoint prediction i.e. weld state 3. Figure 16 reveals that the correlation between energy and kurtosis features varies depending on the weld seam states i.e. weld profile shape. Such interpretation of the feature space hints us with the possibility of classifying the weld seam states and predict the endpoint of weld seam removal.

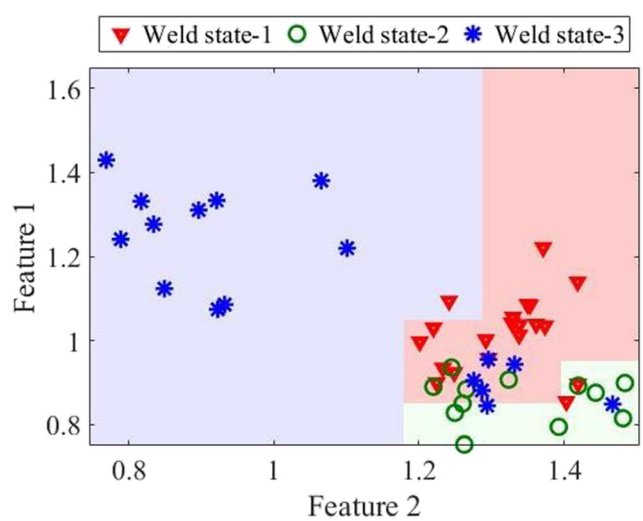

Fig. 17 Support vector machine-based hyperplane for classification from the training set

4.3 Support vector machine-based endpoint detection

In this paper, the weld seam profile geometry evolved at different states 1, 2 and 3 of the belt grinding process which are assigned as discrete classifiers. The proposed SVM training parameters are given in Table 4. Well-chosen kernel function and finest value of parameters for the specific kernel are critical for the performance of the predictive model.

The quadratic kernel function is used for implementations of the classification model, and 30% hold-out validation was performed using MATLAB classification learner Toolbox. Figure 17 exhibits that there is a clear separation drawn by the hyperplane in the feature space between different weld state classifiers.

Performance measure experiment with 30% hold-out and 528-wavelet decomposition features on the quadratic SVM model had an accuracy of prediction of 95.3%. Figure 18 shows a three-by-three confusion matrix for the classification of three different weld states with 95.3% accuracy obtained using the quadratic SVM model with a small fraction of samples misclassified. The proposed approach is composed primarily of three steps. In the first step, discrete classifiers are identified, and the corresponding sensor signatures are preprocessed. In the second step, features are extracted using wavelet decomposition based on Daubechies-4 mother wavelet discussed in Sect. 4.2. In the final step training and classification, exercises are performed on a quadratic kernel-based SVM.

5 Validation of proposed methodology

In industries, weld seam comes in different shape, size, geometry, material filler rod and even locations that are hard to access. To validate the robustness of the proposed methodology, an experimental trial to predict weld seam removal using different weld seam shape, size and geometry profile as shown in Fig. 19a is introduced. The new weld seams are made up of stainless steel (SUS308) filler rod on mild steel work coupons using tungsten inert gas welding similar to that in Sect. 3.3. The dimension of the new weld seam is 20 mm × 12 mm × 0.6 mm (L × B × H) on a flat mild steel work coupon, and a DWT, SVM and multi-sensor integration system is employed. On the proposed methodology, the new weld seam profile specimens were grinded with the same process parameters as discussed in Table 1. The previously developed complementary multi-sensor integration system comprising force and accelerometer was exercised to assess the state of the weld seam removal. Weld seams of three different removal states as illustrated in Fig. 19a, b were grinded with an abrasive belt under the same grinding condition. The signatures during machining of different weld seam states are captured using appropriate force and accelerometer with a sampling rate of 2 kHz as discussed in Sect. 3.1. Based on the sensor readings that were recorded during the grinding process of the new weld seam at states 1, 2 and 3, it is evident that there is a reduction in the magnitude of the signatures for both accelerometer and force sensor, respectively. The orthogonal Daubechies filters of length 4 are applied to extract the wavelet coefficients of discrete time signals as elaborated in Sect. 4.1. The sensor signals obtained during grinding different states of the new weld seam profile geometry are also distinct in wavelet decompositions when they are compared with each other. The Daubechies-4 wavelet function was used to extract features from the sensors with a window size of 20 and spacing of the window of 5. Features discussed in Table 3 are computed using all the coefficients of the details and the final approximation from sensor signatures obtained during grinding of a different weld seam profile.

Features extracted from force and accelerometer is concatenated to form one large vector space of 528 features that is used for endpoint prediction. The new weld seam profile geometry evolved at different states 1, 2 and 3 of the belt grinding process which are assigned as discrete classifiers. Performance measure experiment with 30% hold-out and 528-wavelet decomposition features on the quadratic SVM model had an accuracy of prediction of 93.8%. Figure 20 shows a three-by-three confusion matrix for classification of three different weld states with 93.8% accuracy obtained using the quadratic SVM model with a minimum fraction of samples misclassified. The accuracy of the results from the new weld geometry removal suggests that the proposed methodology using a DWT, SVM and multi-sensor integration system is robust enough to predict complete removal of weld seam from a surface.

True class	Weld state-1	Weld state-2	Weld state-3
Weld state-1	91%		
Weld state-2		95%	
Weld state-3	9%	5%	100%
Positive predicted value	91%	95%	100%
False discovery rate	9%	5%	
	Weld state-1	Weld state-2	Weld state-3

Predicted class

Fig. 18 Confusion matrix depicting classifier performance in weld states 1, 2 and 3

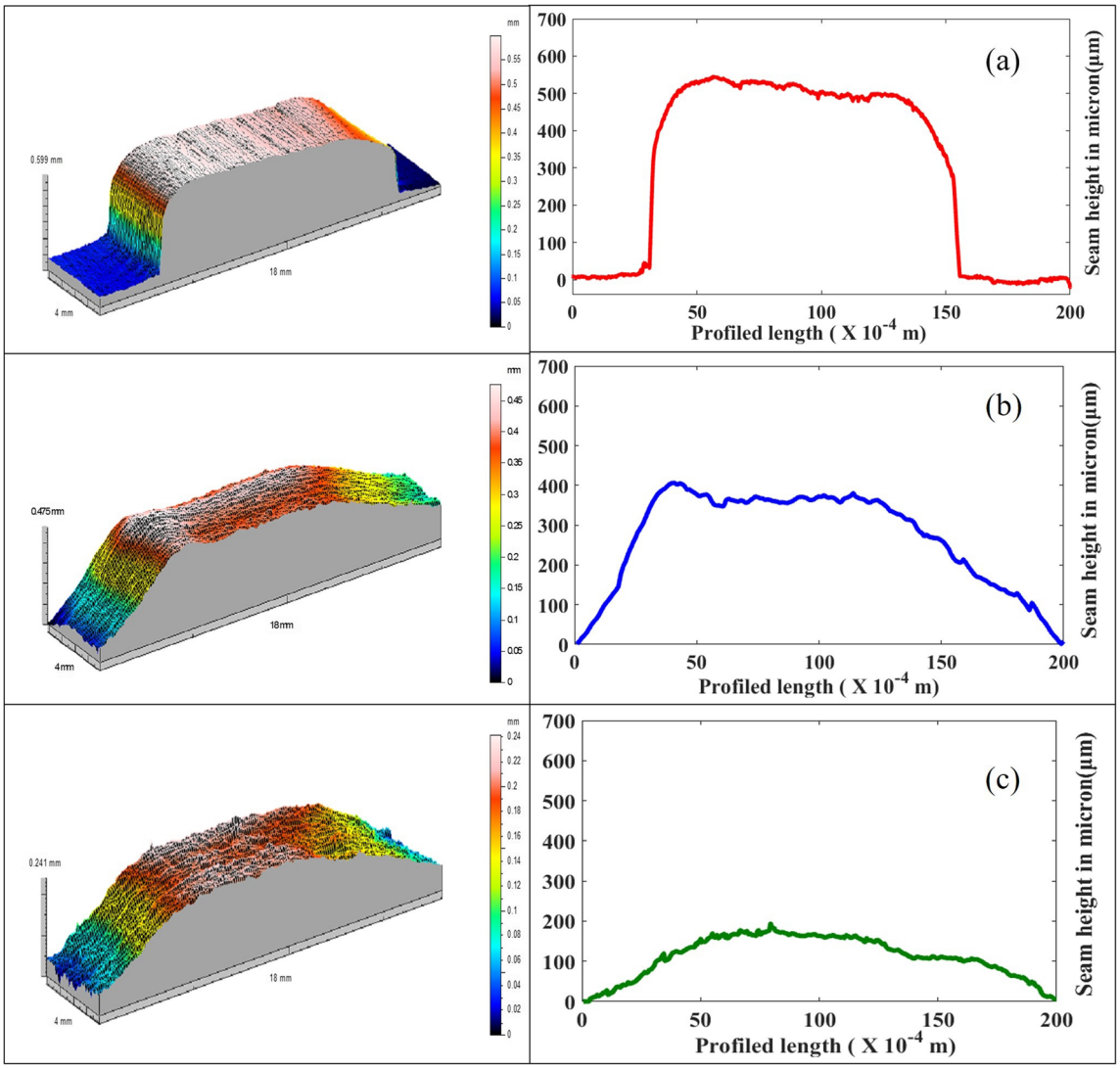

Fig. 19 **a** 3D and 2D profile extracted from the weld seam before belt grinding process. **b** 3D and 2D non-symmetrical profile extracted from the weld seam after consecutive passes of belt grinding process (state 1). **c** 3D and 2D profile extracted when the weld seam is distinctively removed (state 2)

6 Conclusion

In this study, the evolution of the weld seam geomentry at different stages of removal in belt grinding process time is identified, analysed and presented. The paper introduces the use of the wavelet decomposition to predict removal and evolution of weld seams. Based on the experimental results and summarising the research, the following generalised conclusions are drawn:

1 A complementary-based sensor integration approach has been successfully developed to predict weld seam states, and sensor positioning has been accomplished.
2 Transitions in vibration and force signals generated during belt grinding of three different weld seam states are identified.
3 The wavelet features that can possibly correlate weld seam removal status has been identified and deployed along with the machine learning model based on SVM.
4 The study indicated that SVM could classify the estimated parameters of wavelet decomposition accurately. The results demonstrate that the developed diagnostic method is a potential tool to predict endpoint of weld seam removal reliably.
5 The proposed methodology has also been validated with weld seam of different shape, size and geometry to gain confidence in the robustness.

However, this is still a preliminary study, as in industries weld seam comes in complicated geometries, material and even locations that are hard to access. A more robust technique has to be developed to create a model which employs

True class			
Weld state-1	83%		
Weld state-2	17%	100%	
Weld state-3			100%
Positive predicted value	83%	100%	100%
False discovery rate	17%		
	Weld state-1	Weld state-2	Weld state-3

Predicted class

Fig. 20 Confusion matrix depicting classifier performance in weld states 1, 2 and 3 for the new weld seam geometry

optimised feature space, sensor selection, sensor placement and process parameters that would suitably solve a range of problems and is in progress for further research.

Acknowledgements This work was conducted within the Rolls-Royce@NTU Corporate Lab with support from the National Research Foundation (NRF) Singapore under the Corp Lab@University Scheme.

References

1. Islam MU, Xue L, McGregor G (2001) Process for manufacturing or repairing turbine engine or compressor components. U.S. Patent 6,269,540
2. Heitman PW, Hammond SN, Brown LE (1991) Method for joining single crystal turbine blade halves. U.S. Patent 5,071,059
3. Axinte D, Kritmanorot M, Axinte M, Gindy N (2005) Investigations on belt polishing of heat-resistant titanium alloys. J Mater Process Technol 166(3):398–404
4. Ren X, Cabaravdic M, Zhang X, Kuhlenkötter B (2007) A local process model for simulation of robotic belt grinding. Int J Mach Tools Manuf 47(6):962–970
5. (2011) Automated weld seam removal system promises removal rates over 20 times faster than manual grinding. Industrial Robot: An International Journal 38 (4). doi:10.1108/ir.2011.04938daa.002
6. Ito Y (2014) In-process measurement for machining states: sensing technology in noisy space. In: Thought-evoking approaches in engineering problems. Springer International Publishing, Cham, p 17–40. doi:10.1007/978-3-319-04120-9_2
7. Chen JC, Huang L, Lan A, Lee S (1999) Analysis of an effective sensing location for an in-process surface recognition system in turning operations. J Ind Technol 15(3):1–6
8. Chen X, Chen S, Lin T, Lei Y (2006) Practical method to locate the initial weld position using visual technology. Int J Adv Manuf Technol 30(7):663–668. doi:10.1007/s00170-005-0104-z
9. Luo H, Chen X (2005) Laser visual sensing for seam tracking in robotic arc welding of titanium alloys. Int J Adv Manuf Technol 26(9):1012–1017. doi:10.1007/s00170-004-2062-2
10. Luo RC, Kay MG (1990) A tutorial on multisensor integration and fusion. In: Industrial electronics society. IECON'90., 16th Annual Conference of IEEE, 1990. IEEE, p 707–722
11. Dornfeld D (1986) Acoustic emission process monitoring for untended manufacturing. In: Proc. Japan-USA Symposium on Flexible Automation, p 831–836
12. Pandiyan V, Tjahjowidodo T, Samy MP (2016) In-process surface roughness estimation model for compliant abrasive belt machining process. Procedia CIRP 46:254–257
13. Kanish TC, Kuppan P, Narayanan S, Ashok SD (2014) A fuzzy logic based model to predict the improvement in surface roughness in magnetic field assisted abrasive finishing. Procedia Eng 97(Complete):1948–1956. doi:10.1016/j.proeng.2014.12.349
14. Caesarendra W, Kosasih B, Tieu AK, Moodie CAS (2014) Circular domain features based condition monitoring for low speed slewing bearing. Mech Syst Signal Process 45(1):114–138. doi:10.1016/j.ymssp.2013.10.021
15. Kasashima N, Mori K, Ruiz GH, Taniguchi N (1995) Online failure detection in face milling using discrete wavelet transform. CIRP Ann Manuf Technol 44(1):483–487. doi:10.1016/S0007-8506(07)62368-3
16. Xiaoli L (1999) On-line detection of the breakage of small diameter drills using current signature wavelet transform. Int J Mach Tools Manuf 39(1):157–164
17. Learned RE, Willsky AS (1995) A wavelet packet approach to transient signal classification. Appl Comput Harmon Anal 2(3):265–278
18. Nurprasetio P, Bagiasna K, Suharto D, Tjahjowidodo T (2010) The development of a novel fault identification technique by combining minimum-distance pattern-recognition and discrete wavelet transform. In: Proceedings of international conference on intelligent unmanned systems
19. Tansel IN, Mekdeci C, Mclaughlin C (1995) Detection of tool failure in end milling with wavelet transformations and neural networks (WT-NN). Int J Mach Tools Manuf 35(8):1137–1147
20. Saravanan N, Ramachandran K (2010) Incipient gear box fault diagnosis using discrete wavelet transform (DWT) for feature extraction and classification using artificial neural network (ANN). Expert Syst Appl 37(6):4168–4181
21. Azouzi R, Guillot M (1997) On-line prediction of surface finish and dimensional deviation in turning using neural network based sensor fusion. Int J Mach Tools Manuf 37(9):1201–1217
22. Pöyhönen S, Arkkio A, Jover P, Hyötyniemi H (2005) Coupling pairwise support vector machines for fault classification. Control Eng Pract 13(6):759–769
23. Çaydaş U, Ekici S (2012) Support vector machines models for surface roughness prediction in CNC turning of AISI 304 austenitic stainless steel. J Intell Manuf 23(3):639–650. doi:10.1007/s10845-010-0415-2
24. Schölkopf B, Smola AJ (2001) Learning with kernels: support vector machines, regularization, optimization, and beyond. MIT press Cambridge, MA
25. Noble WS (2006) What is a support vector machine? Nat Biotechnol 24(12):1565–1567
26. Zhang X, Kuhlenkötter B, Kneupner K (2005) An efficient method for solving the Signorini problem in the simulation of free-form surfaces produced by belt grinding. Int J Mach Tools Manuf 45(6):641–648
27. Khellouki A, Rech J, Zahouani H (2007) The effect of abrasive grain's wear and contact conditions on surface texture in belt finishing. Wear 263(1):81–87
28. Zhu Z, Yan R, Luo L, Feng Z, Kong F (2009) Detection of signal transients based on wavelet and statistics for machine fault diagnosis. Mech Syst Signal Process 23(4):1076–1097

29. Shukla KK, Tiwari AK (2013) Filter banks and DWT. In: Efficient algorithms for discrete wavelet transform: With applications to denoising and fuzzy inference systems. Springer London, London, pp 21–36. doi:10.1007/978-1-4471-4941-5_2

30. Vapnik V (1998) The support vector method of function estimation. In: Suykens JAK, Vandewalle J (eds) Nonlinear modeling: Advanced black-box techniques. Springer US, Boston, MA, pp 55–85. doi:10.1007/978-1-4615-5703-6_